J. Fluid Mech. (1985), *vol.* 153, *pp.* 401–416
Printed in Great Britain

Friction factors for a lattice of Brownian particles

By ALAN J. HURD†
Martin Fisher School of Physics, Brandeis University, Waltham, Massachusetts 02254

NOEL A. CLARK, RICHARD C. MOCKLER AND WILLIAM J. O'SULLIVAN
Department of Physics, University of Colorado, Boulder, Colorado 80309

(Received 31 August 1984 and in revised form 13 November 1984)

The resistance to oscillatory motions of arbitrary wavelengths in an infinitely dilute lattice of identical spheres, immersed in a viscous fluid, is calculated from the linearized Navier–Stokes equation to lowest order in fluid inertia and sphere-volume fraction. The application we have in mind is to analyse the hydrodynamic modes in colloidal crystals (a lattice of Brownian particles repelling each other electrically), although other applications are possible. We find that the friction per particle for both compressional and transverse shear modes is close to the Stokes value at short wavelengths, whereas at long wavelengths fluid backflow within the lattice is important and causes the friction to increase for compressional modes. For shear modes, in which backflow is not present, the friction decreases from the Stokes value at short wavelengths to zero at long wavelengths. At sufficiently long wavelengths, when the shear-mode friction becomes small enough, propagating viscoelastic modes are possible in a lattice with elastic forces between spheres. Fluid inertia is most important for long-wavelength transverse motions, since a significant amount of fluid mass gets carried along by each particle. Explicit results for a *bcc* lattice are presented along with interpolation formulas, and the pertinence of these results to colloidal crystals is discussed. Finally, the effects of constraining walls are explored by considering a one-dimensional lattice near a wall. Backflow imposed by the wall increases the friction factors for the lattice modes, showing that propagating modes are unlikely in colloidal crystals that are confined to a cell thinner than a critical length.

1. Background: colloidal crystals

It has been shown recently that the lattice dynamics of colloidal crystals, which consist of strongly repelling charged Brownian particles arranged in a lattice, can be described by a harmonic lattice immersed in a viscous medium (Hurd 1981; Hurd *et al.* 1982). A hydrodynamic interaction between the particles arises when the moving particles exchange momentum through the viscous fluid, thereby changing the resistance to particle motion. This effect is of crucial importance to the sedimentation and rheology of concentrated dispersions of colloidal-size particles, but has generally been regarded as being small enough to neglect for the dynamics of sufficiently dilute colloidal systems. Of course, the complexity of the problem has encouraged this neglect. If is difficult to say, for example, when the particle concentration is 'sufficiently dilute', especially since the hydrodynamic interaction depends on the

† Permanent address: Division 1152, Sandia National Laboratories, Albuquerque, NM 87185.

configuration of the particles, but in general the greater the configurational order the greater the importance of the interaction. In this paper, we will discuss highly ordered configurations, such as those found in dilute colloidal crystals, as a special case for which results can be readily obtained.

There are two reasons why the hydrodynamic interaction is more important in a lattice of Brownian particles than in dilute suspensions. First, the Stokes velocity field created by a moving sphere in a fluid decays only as r^{-1}, and, when the effects of many particles are summed, the local fluid velocity in the neighbourhood of a sphere has significant contributions from not just the nearest-neighbour particles, but from particles at all distances as well. The second reason is much more surprising: the regular arrangement of spheres in a lattice causes the hydrodynamic effects to enter at order $\phi^{\frac{1}{3}}$, where ϕ is the volume fraction of the spheres, instead of order ϕ as in a random-free arrangement. This point has been noticed in the sedimentation problem for arrays of spheres, and is related to the existence of a well-defined spatial correlation length in a given configuration (Saffman 1973). Hence 'sufficient dilution' at which hydrodynamic interactions become negligible for an ordered suspension is three orders of magnitude more dilute than for disordered suspensions.

Experimentally, the dynamical response of colloidal crystals has been studied in a number of ways. Thermally excited compressional, or longitudinal, modes in the lattice have been found to be overdamped by dynamic light scattering, whereas shear, or transverse, modes have exhibited overdamped behaviour at short wavelengths and, in thin-film cells, overdamped behaviour at long wavelengths as well (Hurd 1981; Hurd *et al.* 1982). In containers of larger dimensions, however, transverse modes can be underdamped as shown by a variety of mechanical measurements (Pieranski *et al.* 1981; Russel & Benzing 1981; Benzing & Russel 1981; Lindsay & Chaikin 1982). In fact it is quite common to see the 'shimmering' of the Bragg-scattered light from a flashlight illuminating a vial of colloidal crystals as a result of long-wavelength transverse distortions excited by external vibrations. In order to get a clear unified picture of the dynamical responses of such systems, it is necessary to study the role of the solvent-mediated hydrodynamic interactions.

From the solution to the time-dependent Navier–Stokes equation for an incompressible fluid in which a lattice of spheres performs arbitrary small motions, we will show in §2 that the strong damping of longitudinal modes for all wavelengths is due to backflow imposed by 'extended' or 'closed' boundary conditions such as those provided by a wall or the infinite surface area of neighbouring spheres far from a given sphere in an unbounded lattice. Transverse modes, on the other hand, require no backflow (in the absence of walls) in the centre-of-mass frame, and therefore experience a vanishing friction in the limit of long wavelengths, since there is no relative motion between the particles and the fluid.

In order to illustrate exactly what it is we wish to calculate, we first consider a simple harmonic lattice model for a colloidal crystal (Hurd 1981; Hurd *et al.* 1981). While the elastic lattice case may be of limited general interest, it is a good vehicle for introducing the basic concepts and nomenclature of lattice dynamics from solid-state theory, which are invaluable in discussing the problem of hydrodynamic flow around a lattice. Therefore we begin with a lattice of spheres interacting directly through pair potentials and indirectly through the hydrodynamic flow. The equation of motion for the nth sphere can be written as

$$m_0 \ddot{\boldsymbol{x}}_n = -\sum_m \boldsymbol{u}_{mn} \boldsymbol{x}_m - \sum \boldsymbol{w}_{nm} \dot{\boldsymbol{x}}_m + \boldsymbol{X}_n, \tag{1}$$

where $\boldsymbol{x}_n$ is the displacement of sphere n from its equilibrium site, $\boldsymbol{X}_n$ is an external force acting on sphere n, $\boldsymbol{u}_{nm}$ is the force tensor and $\boldsymbol{w}_{nm}$ is the dissipation tensor. The external force is present only to provide a (formal) force to drive the oscillatory motions that we wish to study. In a physical situation it may be a random force, gravity, or any other force acting only on the particles. The tensor $\boldsymbol{u}_{nm}$ gives the force by direct interactions on sphere n for a unit displacement of sphere m, whereas $\boldsymbol{w}_{nm}$ relates the hydrodynamic force on sphere n produced by movement of sphere m. After a normal-modes transformation, $\boldsymbol{x}_n = \Sigma_q \boldsymbol{a}_q \exp[\mathrm{i}\boldsymbol{q}\cdot\boldsymbol{R}_n]$, we get

$$\ddot{\boldsymbol{a}}_q = -\boldsymbol{D}_q \boldsymbol{a}_q \boldsymbol{\Lambda}_q \dot{\boldsymbol{a}}_q + \boldsymbol{X}_q, \tag{2}$$

where $\boldsymbol{D}_q$ is the Fourier transform of the potential tensor $\boldsymbol{u}_{nm}$ and $\boldsymbol{\Lambda}_q$ is the Fourier transform of the dissipation tensor $\boldsymbol{w}_{nm}$:

$$\boldsymbol{D}_q = m_0^{-1} \sum_n \boldsymbol{u}_{n1}\, \mathrm{e}^{\mathrm{i}\boldsymbol{q}\cdot(\boldsymbol{R}_n - \boldsymbol{R}_1)},$$

$$\boldsymbol{\Lambda}_q = m_0^{-1} \sum_n \boldsymbol{w}_{n1}\, \mathrm{e}^{\mathrm{i}\boldsymbol{q}\cdot(\boldsymbol{R}_n - \boldsymbol{R}_1)}.$$

$\boldsymbol{D}_q$ is known in solid-state theory as the dynamical matrix; it contains the information concerning undamped normal-mode frequencies for the system. By analogy, we will call $\boldsymbol{\Lambda}_q$ the 'dissipation matrix' since it contains the information concerning damping of the normal modes, including the friction factors that we seek.

After final diagonalization (the simultaneous diagonalization of $\boldsymbol{D}_q$ and $\boldsymbol{\Lambda}_q$)† and a time Fourier transform, the equations of motion become completely decoupled into three modes (one longitudinal and two transverse), the νth mode obeying a simple, forced-harmonic-oscillator equation

$$a_q^\nu[-\omega^2 + (\omega_q^\nu)^2 - \mathrm{i}\omega\lambda_q^\nu] = X_q^\nu, \tag{3}$$

where $(\omega_q^\nu)^2$, the νth eigenvalue of $\boldsymbol{D}_q$, represents the undamped frequency, and λ_q^ν, the νth eigenvalue of $\boldsymbol{\Lambda}_q$, is the damping or friction factor for the oscillator. In the usual lattice dynamics of solids, the undamped frequency ω_q^ν, considered as a function of $\boldsymbol{q}$, is the phonon dispersion relation giving the frequency (or energy) of a lattice vibration as a function of wavelength of the disturbance in the particle displacements. It will become apparent that, owing to the hydrodynamic interaction, the friction factor has dispersion, i.e. it is a function of $\boldsymbol{q}$, and that it is complex, the imaginary part representing fluid inertia.

From (1), the fluid drag force acting on the nth particle is $-\Sigma_m \boldsymbol{w}_{nm}\dot{\boldsymbol{x}}_m$. By action–reaction, the fluid experiences equal and opposite forces at the particle sites, each of which can be decomposed into a set of independent contributions from each normal mode. In §2 we find the relation between these normal-mode contributions and the particle velocities; the proportionality constants are the friction factors λ_q^ν. Section 3 deals with the effects of unsteady flow and how the effective mass of the

† Final diagonalization is a simple rotation of axes to decouple the spatial components of the normal modes. The simultaneous diagonalization of $\boldsymbol{D}_q$ and $\boldsymbol{\Lambda}_q$ by a rotation matrix is possible only if $\boldsymbol{D}_q$ and $\boldsymbol{\Lambda}_q$ commute and at least one of them is positive definite (see Noble 1969). The dissipation matrix is positive definite since its quadratic form is just one-half the dissipated energy, but commutativity does not seem to be guaranteed for general directions of the wave vector $\boldsymbol{q}$. For the special high-symmetry directions of $\boldsymbol{q}$ considered here, however, commutativity holds. One could argue further that, within the context of a linearized theory with only pair interactions, no mode coupling can exist; there can be no coupling between longitudinal and transverse flows. For arbitrary directions of $\boldsymbol{q}$ there are no purely longitudinal or transverse modes; nevertheless there must be three uncoupled modes.

coupled sphere–fluid modes is increased by fluid inertia. These effects are further discussed for an elastic lattice, such as a colloidal crystal, in §4. Finally, in §5, the qualitative effects of walls are determined by considering a one-dimensional chain of beads on a lattice near a wall with Oseen interactions. The main result of this section is that the extended boundary conditions of the wall impose a backflow that suppresses propagating modes in the chain. In a similar way, propagating modes in a three-dimensional colloidal crystal would be suppressed in sample cells smaller than a critical wavelength, consistent with recent data (Hurd 1981; Hurd *et al.* 1982).

2. Lattice hydrodynamics

First it is necessary to calculate the fluid velocity flowing around a dilute lattice of identical particles that are performing small-amplitude motions about their lattice sites. Rotational motions and their coupling to translations are neglected for simplicity; also, since they involve higher moments of the forces induced by the spheres on the fluid, they result in corrections of a higher order in volume fraction (Happel & Brenner 1973). The solution requires only a reasonable modification of Hasimoto's (1959) calculation for a sedimenting perfect lattice, using the method of induced forces. Indeed, the result in this section can be viewed as a case with special symmetry of more general many-sphere calculations for arbitrary configurations using the induced-forces technique (Mazur 1982; van Saarloos & Mazur 1983). The general procedure is to calculate the force on a representative sphere in the lattice by replacing all the others by forces acting on the fluid, where each force is acting in a way appropriate for the modes present (that is, each sphere exerts a force that is the superposition of forces for each normal-mode disturbance in the lattice), then to satisfy the boundary conditions on the representative sphere. The finite sizes of the other spheres can be neglected since they introduce a correction of order ϕ, and we are interested in a theory of order $\phi^{\frac{1}{3}}$. Hence we assume point forces on the fluid. Also, the point forces are assumed to act precisely at the lattice sites, ignoring the finite displacements of the particles. This approximation is also consistent with a harmonic lattice theory.

As a point of reference, we know that the friction factor Hasimoto obtained for a body-centred cubic lattice sedimenting in the [100] direction (normal to a face of a bcc cubic unit cell) is the asymptotic value we should find for a [100] longitudinal mode as the wavelength increases to infinity. That value is

$$\lambda^L_{q100} = \lambda_0[1-1.792\phi^{\frac{1}{3}}+O(\phi)]^{-1}, \tag{4}$$

where $\lambda_0 = 6\pi\eta a/m_0$, ϕ is the volume fraction of spheres and m_0 the mass of a sphere.

The unsteady Stokes equation for an incompressible fluid under the action of forces $\boldsymbol{F}$ is

$$-\rho\dot{\boldsymbol{v}} = \nabla\rho-\eta\nabla^2\boldsymbol{v}-\boldsymbol{F}, \tag{5}$$

along with

$$\nabla\cdot\boldsymbol{v} = 0, \tag{6}$$

and, for this problem, stick boundary conditions on the surface of each sphere.

By eliminating the pressure and solving for $\boldsymbol{v}$ using Fourier transforms, we obtain the well-known equation

$$\boldsymbol{v}(\boldsymbol{k},\omega) = \eta^{-1}(k^2+k_0^2)^{-1}\left[\boldsymbol{F}-\frac{\boldsymbol{k}(\boldsymbol{k}\cdot\boldsymbol{F})}{k^2}\right], \tag{7}$$

where $k_0^2 = -i\omega\rho/\eta$. The last result is the fundamental solution for arbitrary forces acting on the fluid.

In reality, the induced forces $\boldsymbol{F}$ act on the spherical shells of the fluid that contact the particles' surfaces. Saffman (1973) has shown that these forces may be replaced by their monopole moments, with an error of order ϕ. With this approximation, the forces on the fluids are

$$\boldsymbol{F}(\boldsymbol{r}, t) = m_0 \sum_n \boldsymbol{f}_n(t)\, \delta^3(\boldsymbol{r} - \boldsymbol{R}_n), \tag{8}$$

where $\boldsymbol{f}_n(t)$ is the point force per unit mass exerted by the nth sphere at its lattice site $\boldsymbol{R}_n$. We assume that the force exerted by sphere n can be formally decomposed into normal-mode contributions,

$$\boldsymbol{f}_n(t) = \sum_q \boldsymbol{f}_q(t)\, e^{i\boldsymbol{q}\cdot\boldsymbol{R}_n}, \tag{9}$$

so that the Fourier transform of the body forces $\boldsymbol{F}$ is

$$\mathbb{F}(\boldsymbol{k}, \omega) = (2\pi)^3 m_0 \Omega^{-1} \sum_q \boldsymbol{f}_q(\omega) \sum_m \delta^3(\boldsymbol{k} - (\boldsymbol{K}_m + \boldsymbol{q})). \tag{10}$$

Here Ω is the volume of a space lattice unit cell, the set $\{\boldsymbol{K}_m\}$ is the set of reciprocal lattice vectors (which make up the spatial Fourier transform of the direct lattice) and the following formula has been used:

$$\sum_n e^{-i(\boldsymbol{k}-\boldsymbol{q})\cdot\boldsymbol{R}_n} = \frac{(2\pi)^3}{\Omega} \sum_m \delta^3(\boldsymbol{k} - (\boldsymbol{K}_m + \boldsymbol{q})).$$

Owing to the lattice periodicity, the normal-mode wave vector $\boldsymbol{q}$ may be considered to be confined to the Wigner–Seitz unit cell of the reciprocal lattice, the so-called first Brillouin zone, without loss of information. The Brillouin zone around a lattice site is defined as all of the points in reciprocal space that are closer to that site than any other lattice site. Each site is therefore enclosed by a polyhedral box formed by planes midway between other reciprocal lattice sites. A mode whose wave vector $\boldsymbol{q}$ extends beyond the zone boundary to the mth reciprocal lattice unit cell is equivalent to a mode whose wave vector is $\boldsymbol{q} - \boldsymbol{K}_m$, which lies in the first Brillouin zone, because the factor $\exp(i\boldsymbol{q}\cdot\boldsymbol{R}_n)$ repeats as $\boldsymbol{q}$ extends beyond the first zone boundary.

Substituting the last expression into (7) and transforming to the $(\boldsymbol{r}, \omega)$-representation gives

$$v^\alpha(\boldsymbol{r}, \omega) = \frac{m_0}{\Omega\eta} \sum_q f_q^\beta(\omega) \sum_m \frac{e^{iK'_m\cdot r}}{K'^2_m + k_0^2} \left(\delta^{\alpha\beta} - \frac{K'^\alpha_m K'^\beta_m}{K'^2_m}\right), \tag{11}$$

where $\boldsymbol{K}' = \boldsymbol{K} + \boldsymbol{q}$. This is the solution for the fluid velocity induced by point forces on a perturbed lattice. Certain higher-order spatial derivatives of (7) are also solutions, but these enter at higher order in ϕ.

By action-reaction, the induced body forces $\boldsymbol{f}_q$ act back on the particles as drag forces. Substituting the nth particle velocity $\boldsymbol{x}_n = \sum \boldsymbol{a}_q \exp(i\boldsymbol{q}\cdot\boldsymbol{R}_n)$ into the total drag force $-\sum \boldsymbol{w}_{nm}\dot{\boldsymbol{x}}_m$, and equating each normal-mode component to $-\boldsymbol{f}_q$, we find

$$m_0 f_q^\alpha = \Lambda_q^{\alpha\beta} \dot{a}_q^\beta. \tag{12}$$

Meanwhile, the fluid boundary condition at the nth sphere's surface is satisfied (consistent to the degree of approximation at hand) by equating the particle velocity

Direction	Q	Symmetry points	κ_q^{xx}	κ_q^{xy}	κ_q^{yy}	κ_q^{zz}
[100]	0.0	Γ	1.792	0.000	1.792	1.792
	0.05	—	1.789	0.000	1.791	1.791
	0.10	—	1.780	0.000	1.788	1.788
	0.15	—	1.765	0.000	1.783	1.783
	0.20	—	1.744	0.000	1.776	1.776
	0.25	—	1.716	0.000	1.768	1.768
	0.30	—	1.682	0.000	1.759	1.759
	0.35	—	1.641	0.000	1.748	1.748
	0.40	—	1.594	0.000	1.736	1.736
	0.45	—	1.541	0.000	1.724	1.724
	0.50	—	1.483	0.000	1.711	1.711
	0.55	—	1.421	0.000	1.697	1.697
	0.60	—	1.356	0.000	1.683	1.683
	0.65	—	1.290	0.000	1.667	1.667
	0.70	—	1.225	0.000	1.650	1.650
	0.75	—	1.165	0.000	1.630	1.630
	0.80	—	1.110	0.000	1.608	1.608
	0.85	—	1.065	0.000	1.582	1.582
	0.90	—	1.031	0.000	1.552	1.552
	0.95	—	1.009	0.000	1.515	1.515
	1.00	H	1.002	0.000	1.472	1.472
[111]	0.00	Γ	1.792	0.000	1.792	1.792
	0.05	—	1.791	0.000	1.791	1.791
	0.10	—	1.787	0.000	1.787	1.787
	0.15	—	1.781	0.001	1.781	1.781
	0.20	—	1.772	0.001	1.772	1.772
	0.25	—	1.760	0.001	1.760	1.760
	0.30	—	1.746	0.001	1.746	1.746
	0.35	—	1.729	0.000	1.729	1.729
	0.40	—	1.709	−0.002	1.709	1.709
	0.45	—	1.687	−0.006	1.687	1.687
	0.50	P	1.661	−0.012	1.661	1.661
	0.55	—	1.632	−0.020	1.632	1.632
	0.60	—	1.601	−0.030	1.601	1.601
	0.65	—	1.567	−0.043	1.567	1.567
	0.70	—	1.530	−0.059	1.530	1.530
	0.75	—	1.491	−0.078	1.491	1.491
	0.80	—	1.450	−0.100	1.450	1.450
	0.85	—	1.407	−0.125	1.407	1.407
	0.90	—	1.364	−0.152	1.364	1.364
	0.95	—	1.321	−0.180	1.321	1.321
	1.00	H	1.278	−0.209	1.278	1.278
[110]	0.00	Γ	1.792	0.000	1.792	1.792
	0.05	—	1.791	0.000	1.791	1.791
	0.10	—	1.788	0.000	1.788	1.790
	0.15	—	1.783	0.001	1.783	1.787
	0.20	—	1.776	0.002	1.776	1.783
	0.25	—	1.767	0.004	1.767	1.778
	0.30	—	1.757	0.006	1.757	1.772
	0.35	—	1.744	0.008	1.744	1.763
	0.40	—	1.730	0.012	1.730	1.752
	0.45	—	1.714	0.017	1.714	1.739
	0.50	—	1.697	0.023	1.697	1.724
	0.55	—	1.678	0.030	1.678	1.705

TABLE 1. (*cont. on facing page*).

TABLE 1. (*cont.*)

Direction	Q	Symmetry points	κ_q^{xx}	κ_q^{xy}	κ_q^{yy}	κ_q^{zz}
[110]	0.60	—	1.657	0.040	1.657	1.682
	0.65	—	1.634	0.054	1.634	1.654
	0.70	—	1.609	0.066	1.609	1.622
	0.85	—	1.582	0.084	1.582	1.583
	0.80	—	1.553	0.105	1.553	1.538
	0.85	—	1.521	0.131	1.521	1.485
	0.90	—	1.486	0.162	1.486	1.422
	0.95	—	1.447	0.198	1.447	1.348
	1.00	N	1.403	0.241	1.403	1.262

TABLE 1. Lattice sum $\kappa_q^{\alpha\beta}$ for q in three directions in a *bcc* lattice. The quantity Q is the value of q expressed as a fraction of the zone-boundary wave vector for [100] and [110], and as a fraction of twice the zone boundary wave vector for [111]. The symmetry points are labelled according to the standard scheme.

Direction	α, β	$a_0^{\alpha\beta}$	$a_1^{\alpha\beta}$	$a_2^{\alpha\beta}$	$a_3^{\alpha\beta}$	$a_4^{\alpha\beta}$
[100]	x, x	1.7921	−0.0350	−0.7452	−1.6889	1.6812
	x, y	0.0000	0.0000	0.0000	0.0000	0.0000
	y, y	1.7908	0.0507	−0.8017	1.0940	−0.6607
	z, z	1.7908	0.0507	−0.8017	1.0940	−0.6607
[110]	x, x	1.7912	0.0261	−0.5778	0.4264	−0.2622
	x, y	0.0003	−0.0107	0.1196	−0.1633	0.2948
	y, y	1.7912	0.0261	−0.5778	0.4264	−0.2622
	z, z	1.7912	0.0255	−0.3719	0.3820	−0.5642
[111]	x, x	1.7926	−0.0300	−0.2761	−0.5523	0.3436
	x, y	0.0013	−0.0527	0.4193	−0.8857	0.3075
	y, y	1.7926	−0.0300	−0.2761	−0.5523	0.3436
	z, z	1.7026	−0.0300	−0.2761	−0.5523	0.3436

TABLE 2. Coefficients for polynomial approximations to $\kappa_q^{\alpha\beta}$ using $\kappa_q^{\alpha\beta} = a_0^{\alpha\beta} + a_1^{\alpha\beta} Q + a_2^{\alpha\beta} Q^2 + a_3^{\alpha\beta} Q^3 + a_4^{\alpha\beta} Q^4$

with the surface average of the fluid velocity over a sphere centred at the lattice site with the particle's radius a, $\dot{x}_n = \langle v(r, \omega) \rangle_n$, yielding

$$\dot{a}_q^{\beta} = \frac{m_0}{\Omega\eta} f_q^{\alpha} \sum_m \frac{\langle e^{iK'_m \cdot r} \rangle}{K'^2_m - k_0^2} \left(\delta^{\alpha\beta} - \frac{K'^{\alpha}_m K'^{\beta}_m}{K'^2_m} \right). \tag{13}$$

We note that the act of surface averaging renders $\exp(i\boldsymbol{K}'_m \cdot \boldsymbol{r})$ real, since only the even part (cosine) survives the integration over the surface of a sphere. On comparing (12) and (13), the dissipation matrix can be immediately identified as the inverse of the lattice sum:

$$(\Lambda_q^{-1})^{\alpha\beta} = \frac{m_0}{\Omega\eta} \sum_m \frac{\langle e^{iK'_m \cdot r} \rangle}{K'^2_m + k_0^2} \left(\delta^{\alpha\beta} - \frac{K'^{\alpha}_m K'^{\beta}_m}{K'^2_m} \right). \tag{14}$$

It is convenient at this stage to isolate the fluid inertial (imaginary) part of $\boldsymbol{\Lambda}_q^{-1}$, which will be discussed in §3, from the dissipative (real) part. Also, with the $m = 0$ term written separately, the dissipative part takes the form $\mathrm{Re}\,(\boldsymbol{\Lambda}_q^{-1}) = \boldsymbol{S}_q + \boldsymbol{Y}_q$, where

$$S_q^{\alpha\beta}(\omega) = \frac{m_0}{\Omega\eta} \sum_{m \neq 0} \frac{K_m'^2 \langle e^{iK_m' \cdot r} \rangle}{K_m'^4 - k_0^4} \left(\delta^{\alpha\beta} - \frac{K_m'^\alpha K_m'^\beta}{K_m'^2} \right) \tag{15}$$

and

$$Y_q^{\alpha\beta}(\omega) = \frac{m_0}{\Omega\eta} \frac{q^2 \langle e^{iq \cdot r} \rangle}{q^4 - k_0^4} \left(\delta^{\alpha\beta} - \frac{q^\alpha q^\beta}{q^2} \right). \tag{16}$$

Note that $\boldsymbol{Y}_q$ contributes only to transverse modes and that in these modes it dominates $\boldsymbol{S}_q$ at small q. We will see later that $\boldsymbol{Y}_q$ is responsible for decreasing the friction to transverse motions, allowing them to propagate in a lattice with elastic restoring forces.

Now, if $\omega^2 \ll \omega_0^2 \phi^{\frac{4}{3}}$, where $\omega_0 = \eta/\rho a^2$, then k_0^4 can be ignored in (15), so that the lattice sum can be reduced by the Ewald technique (Hasimoto 1959) to the following form to lowest order in ϕ:

$$S_q^{\alpha\beta} = \lambda_0^{-1} (\delta^{\alpha\beta} - \kappa_q^{\alpha\beta} \phi^{\frac{1}{3}}), \tag{17}$$

where $\kappa_q^{\alpha\beta}$ contains rapidly convergent sums:

$$\begin{aligned} \kappa_q^{\alpha\beta} = {} & \left(\frac{81}{32\pi} \right)^{\frac{1}{3}} \left\{ \delta^{\alpha\beta} + \frac{\gamma(1, z^2 q^2)}{z^2 q^2} \left(\delta^{\alpha\beta} - \frac{q^\alpha q^\beta}{q^2} \right) + \frac{q^\alpha q^\beta}{q^2} e^{-z^2 q^2} \right. \\ & - \sum_{n \neq 0} e^{iq \cdot R_n} \left[\left(\frac{R_n}{2z} \right)^\alpha \left(\frac{R_n}{2z} \right)^\alpha \Phi_{\frac{1}{3}} \left(\left| \frac{R_n}{2z} \right|^2 \right) + \tfrac{1}{2} \delta^{\alpha\beta} \Phi_{-\frac{1}{3}} \left(\left| \frac{R_n}{2z} \right|^2 \right) \right] \\ & \left. + \sum_{m \neq 0} [(zK_m')^\alpha (zK_m')^\beta \Phi_1(|zK_m'|^2) - \delta^{\alpha\beta} \Phi_0(|zK_m'|^2)] \right\}. \end{aligned} \tag{18}$$

Here $z = (8\pi)^{-\frac{1}{3}} \Omega^{\frac{1}{3}}$, $\Phi_\nu(x)$ is the incomplete gamma function,

$$\Phi_\nu(x) = \int_1^\infty \omega^\nu e^{-x\omega} \, d\omega,$$

and $\gamma(n, x)$ is the complementary incomplete gamma function. The physical significance of the quantities κ_q can be seen from (17). The friction factors that we wish to obtain are the eigenvalues of $(\boldsymbol{S}_q + \boldsymbol{Y}_q)^{-1}$, which for a longitudinal mode will look something like $\lambda_q = \lambda_0 (1 - \kappa_q \phi^{\frac{1}{3}})^{-1}$. Thus the elements of κ_q are wavelength-dependent coefficients of the correction to Stokes' law owing to backflow in finite concentrations: a larger κ_q indicates a larger friction and a stronger backflow.

We have calculated $\kappa_q^{\alpha\beta}$ for $\boldsymbol{q}$ extending along the [100], [110] and [111] directions in a *bcc* (space) lattice for 20 points in the Brillouin zone; the results are shown in table 1. Actually, the [111] sum was carried beyond the Brillouin-zone boundary by following an edge between unit cells adjacent to the first zone. Special labels are commonly used for points of special symmetry in the reciprocal lattice: for a face-centred cubic cell (which is reciprocal to *bcc*) Γ is used for the centre of the zone and P, N and H for the most-remote points along the [111], [110] and [100] directions respectively.

In order to simplify calculations, each of the tabulations of $\kappa_q^{\alpha\beta}$ have been approximated by a fourth-order polynomial; the coefficients are shown in table 2. The polynomial expressions are merely convenient contractions of table 1, suitable for interpolation and accurate to better than 0.1 %. Otherwise, the interpolation coefficients have little physical significance.

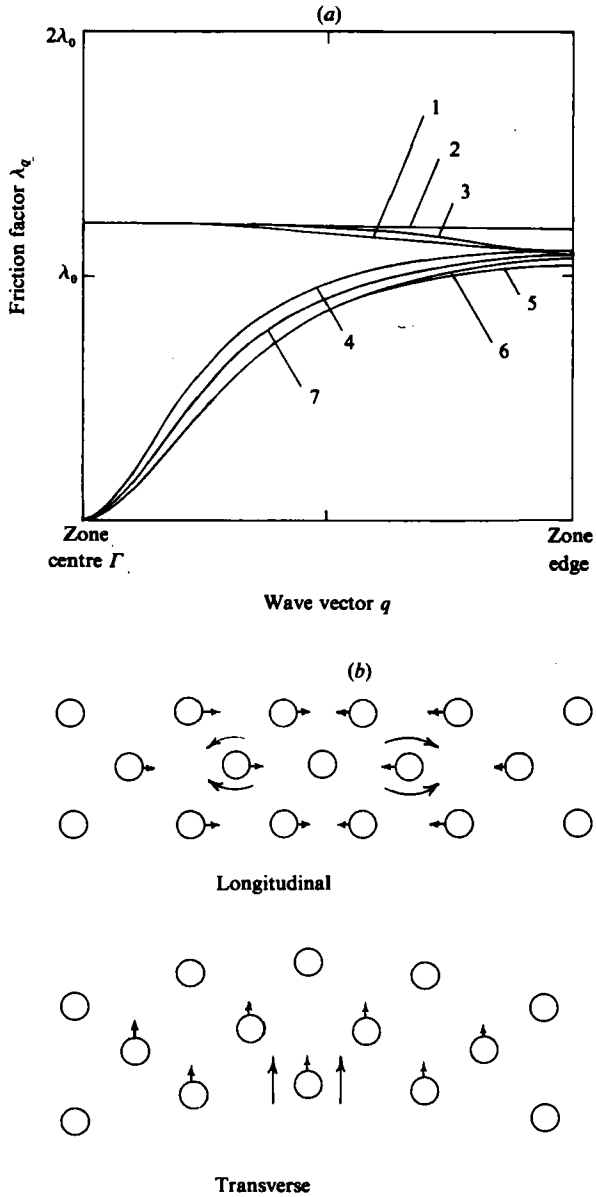

FIGURE 1. (*a*) Friction factors for phononlike modes in a dilute *bcc* lattice for various simple directions and polarizations: (1) [100] longitudinal, (2) [110] longitudinal, (3) [111] longitudinal, (4) [100] transverse, (5) [110] transverse-polarized along [001], (6) [110] transverse-polarized along $[1\bar{1}0]$, (7) [111] transverse. The two transverse modes for [100] and for [111] are degenerate. Contrast the dramatic decrease in friction for transverse modes, which have no backflow, with the increase in friction as the result of backflow effects for longitudinal modes as the wave vector decreases. The friction dispersion curves are plotted from the centre of the Brillouin zone to the zone edge for [100] and [110] (curves 1, 5, and 6), and for [111] beyond the zone edge symmetry point P, which occurs halfway along the abscissa, to the symmetry point H. (Sphere volume fraction $\phi = 0.001$.) (*b*) Schematic of modes along [100]. The first shows the relative displacements of spheres in a longitudinal mode, corresponding to curve (1) in (*a*), and the second shows the displacements in a transverse mode polarized in the [001] direction, corresponding to curve (4).

Using (16), (17) and table 1, the inverse dissipation matrix in (14) may be constructed. It may then be inverted and the eigenvalues found in order to obtain the friction factors. In the [100] direction, for example, we find

$$\lambda^{\mathrm{L}}_{q100} = \lambda_0[1-\kappa^{xx}_q \phi^{\frac{1}{3}}]^{-1}, \tag{19}$$

$$\lambda^{\mathrm{T}}_{q100} = \lambda_0\left[1-\kappa^{yy}_q \phi^{\frac{1}{3}}+\left(\frac{81}{32\pi}\right)^{\frac{1}{3}}\phi^{\frac{1}{3}}(zq)^{-2}\right]^{-1}, \tag{20}$$

where the friction factors for the longitudinal and transverse modes are λ^{L}_q and λ^{T}_q respectively. There are two transverse modes, which remain mutually degenerate throughout the zone and also become degenerate with the longitudinal mode at the symmetry point H as expected. One may verify that at $\boldsymbol{q} = 0$ the longitudinal mode friction is identical with Hasimoto's value in (4). This is the correct result for steady sedimentation in which there are no inertial (finite-frequency) effects.

Figure 1 shows the dispersion of several friction factors through the zone for a volume fraction of $\phi = 0.001$. Note the dramatic decrease in the friction for transverse modes as the wavelength increases. The backflow effect for longitudinal modes shows up as a maximum in the friction near the zone centre (infinite wavelength), at which in each of the three directions shown the longitudinal-mode friction factors have the same value. At the zone boundary, however, where neighbouring spheres move in opposition, the lattice is less isotropic: compressional waves along [110] experience a greater friction than along [100] or [111].

3. Fluid inertia

Returning to (14), the fluid inertia can now be discussed. The imaginary part of the lattice sum $\boldsymbol{\Lambda}_q^{-1}$ separates as the real part does into a purely transverse part $\boldsymbol{Y}'_q$ and the rest of the sum $\boldsymbol{S}'_q$, yielding

$$S'^{\alpha\beta}_q = -\frac{m_0}{\Omega\eta}\sum_{m\neq 0}\frac{k_0^2\langle e^{\mathrm{i}\boldsymbol{K}'_m\cdot\boldsymbol{r}}\rangle}{K'^4_m-k_0^4}\left(\delta^{\alpha\beta}-\frac{K'^{\alpha}_m K'^{\beta}_m}{K'^2_m}\right), \tag{21}$$

$$Y'^{\alpha\beta}_q = -\frac{m_0}{\Omega\eta}\frac{k_0^2\langle e^{\mathrm{i}\boldsymbol{q}\cdot\boldsymbol{r}}\rangle}{q^4-k_0^4}\left(\delta^{\alpha\beta}-\frac{q^\alpha q^\beta}{q^2}\right). \tag{22}$$

We expect $\boldsymbol{Y}'_q$ to dominate the inertial part for small $\boldsymbol{q}$ just as $\boldsymbol{Y}_q$ dominates the dissipative part of $\boldsymbol{\Lambda}_q^{-1}$. We will show that this leads to a higher effective mass for long-wavelength transverse modes as a result of the mass of solvent that gets carried along with the particles. There is a less significant, yet finite, additional mass for longitudinal modes.

For $(zq)^4 \ll 1$, $\boldsymbol{S}'_q$ is negligible compared with $\boldsymbol{Y}'_q$, so that the imaginary part of the transverse-mode friction takes the simple form (in the [100] direction, for example)

$$\lambda'^{\mathrm{T}}_{q100} = \lambda_0\left(\frac{32\pi}{81}\right)^{\frac{1}{3}}\phi^{-\frac{1}{3}}(zk_0)^2 = -\mathrm{i}\omega\phi_m^{-1}, \tag{23}$$

where ϕ_m is the ratio of the mass of a sphere to that of a unit cell of fluid. Substitution into (3) reveals that the fluid-inertia term has the same ω-dependence as the particle-inertia term and that the original quasistatic problem can be recovered by replacing the particle mass m_0 by

$$m_0 \rightarrow m_0(1+\phi_m^{-1}) = m_0 + m_{\mathrm{f}}, \tag{24}$$

where m_{f} is the fluid mass per unit cell. Thus, at sufficiently long wavelengths, the effective mass of the mode is the entire mass of a unit cell, including both the fluid

and the sphere. This is not unexpected, since the fluid and particles move synchronously in these modes.

Similarly, by expanding (21) for small ϕ using the Ewald technique, one can show that for longitudinal modes the imaginary eigenvalues analogous to (23) are of order $-i\omega\phi_m^{-\frac{1}{3}}$ for all q. The longitudinal effective mass is therefore of order $m_0\,\phi_m^{-\frac{1}{3}}$, which, although small compared with the transverse-mode mass, is much larger than m_0, showing that part of the fluid mass in a unit cell is accelerated along with the spheres in a longitudinal mode, the rest participating in the backflow.

Finally, the single oscillating sphere limit can be recovered from the results in §2 if care is taken in proceeding to the limit of an infinite lattice parameter. The discrete lattice sums are not well configured to obtain finite frequency results in the continuum limit, since the expansion parameter $k_0 = (-i\omega\rho/\eta)^{\frac{1}{2}}$ cannot be considered small in comparison with any characteristic wave vectors of the lattice as $R_0 \to \infty$. Instead, it is better to return to (14) and convert the summation over discrete wave vectors (for a long-wavelength longitudinal mode ($q = 0$)) to an integral. (The long-wavelength limit for transverse modes is a linear shear of the lattice, or, in the continuum limit, a single particle in a linear shear field.) The result is

$$\lambda^{\mathrm{L}}_{\text{one sphere}} = \lambda_0(1 - k_0 a + \ldots)^{-1},$$

which is correct in its leading term (Mazur & Bedeaux 1974). Higher-order corrections in frequency can be obtained only by treating the volume of the fluid displaced by the particles more carefully than is done in the point-force method.

4. Elastic lattice

The importance of hydrodynamic interactions between spheres that interact directly by other means is best appreciated by examining the dispersion relations for elastic lattice vibrations. As a physical example, we have in mind colloidal crystals, the particles of which interact electrostatically forming a visco-elastic lattice whose dispersion relations can be measured directly by light scattering. The interactions between neighbouring particles in a colloidal crystal are of order kT, which implies that the separations are only a few Debye lengths. The equivalent hard-sphere diameter for thermodynamic purposes implies that the lattice is electrostatically concentrated, while hydrodynamically it can remain dilute.

Let us continue discussion of the [100] transverse mode in a *bcc* lattice. From (3), (20) and (23), one obtains the complex amplitude of the mode relative to the driving force as

$$\frac{a_q^{\mathrm{T}}}{X_q^{\mathrm{T}}} = [\omega^2 + i\omega(\lambda^{\mathrm{T}}_{q100} + \lambda'^{\mathrm{T}}_{q100}) - (\omega_q^{\mathrm{T}})^2]^{-1} = \phi_m\left[\omega^2 + i\omega\left(\frac{\eta}{\rho}q^2\right) - (Vq)^2\right]^{-1}. \tag{25}$$

In the acoustic (long-wavelength) regime for the purely elastic lattice, the mode's frequency is proportional to the wave vector $\omega_q^{\mathrm{T}} = (k_1/3m_0)^{\frac{1}{2}} R_0\, q = \phi^{\frac{1}{2}} Vq$, with k_1 the effective spring constant between nearest-neighbour spheres and $V = (k_1/3m_{\mathrm{f}})^{\frac{1}{2}} R_0$ the velocity of sound. Equation (25) exhibits the same power spectrum as the shear waves in colloidal crystals considered by Joanny (1979). This can be seen by examining the complex poles $\omega_\pm$ of the above expression. With a little algebra, one finds that the poles must satisfy the dispersion relation

$$q = \frac{\omega_\pm / V}{[1 \pm i\omega_\pm(\eta/\rho V)]^{\frac{1}{2}}}, \tag{26}$$

which is Joanny's result.

A more useful way to analyse (25) is through the Fourier transform of the power spectrum, because it yields a correlation function that can be measured directly by light scattering (Hurd 1981; Hurd *et al.* 1982). A heterodyne experiment at a scattering wave vector $\boldsymbol{k}$, nearer a particular reciprocal lattice vector $\boldsymbol{K}$ than any other, measures the time autocorrelation function of the amplitude of the qth normal mode, $\langle a_q^*(0)\, a_q(t)\rangle$, where $\boldsymbol{q}$ is a reduced wave vector defined by $\boldsymbol{q} = \boldsymbol{k} - \boldsymbol{K}$. It is of the form $\exp(\mathrm{i}\omega_\pm t)$, and the poles are given by

$$\omega_\pm = \mathrm{i}(\tfrac{1}{2}\lambda_q^\nu)\{1 \pm [1 - (2\omega_q^\nu/\lambda_q^\nu)^2]^{\frac{1}{2}}\}.$$

Thus the autocorrelation function, which is the Fourier transform of the power spectrum in (25), has an overdamped, exponentially decaying, form for $\lambda_q^\nu < 2\omega_q^\nu$, and an underdamped, decaying oscillation for $\lambda_q^\nu > 2\omega_q^\nu$. In transverse modes of an infinite lattice, the latter condition is guaranteed to occur at sufficiently small $\boldsymbol{q}$ since λ_q^ν approaches the zone centre quadratically with $\boldsymbol{q}$ (e.g. (20)), whereas ω_q^ν is linear with $\boldsymbol{q}$, being in the acoustic regime. For the [100] mode in a colloidal crystal, the critical wavelength at which this happens is $q_c^{-1} = \eta/2\rho V \approx 30\ \mu\mathrm{m}$. (Here we have used $k_1 = 10^{-3}$ dyn cm^{-1} and $R_0 = 1.5\ \mu\mathrm{m}$ from Hurd *et al.* (1982). Note the error in (32) of Hurd *et al.*, which should read $V = \frac{1}{2}\omega_0 R_0 \phi_m^{\frac{1}{3}}$.) Only those transverse modes whose wavelengths are longer than q_c^{-1} can be expected to show the oscillatory signature of propagation. It is therefore difficult to observe this phenomenon in thin-film samples of the type often used for colloidal-crystal studies. In fact, owing to wall effects discussed in §4, sample vessels much larger than q_c^{-1} must be used to see propagating thermal modes, since in the presence of walls the transverse mode friction is not necessarily small for any $\boldsymbol{q}$.

5. Wall effects

In this section we will analyse the backflow imposed by a single wall on the oscillatory motions of a one-dimensional array of spheres in order to understand better the effects of thin-film sample cells. Hydrodynamic wall effects have been a point of recent interest for sedimentation problems (Goren 1983; Beenakker & Mazur 1984). The backflow imposed by a wall is not the same as the backflow discussed in §2, which was a result of upstream pressure gradients, but the two are related in the sense that both effects are the consequence of 'extended' or 'closed' boundary conditions. (In an infinite array, the particle surfaces constitute a boundary condition of infinite extent, much the same as a wall). The effect of a wall can be readily calculated to first order by the method of reflections using Lorentz's Reciprocal Theorem (Happel & Brenner 1973): given any velocity field $\boldsymbol{v} = (u, v, w)$ and pressure p that satisfy Stokes' equations, Lorentz showed that a new velocity field $\boldsymbol{v}'' = (u'', v'', w'')$ and pressure p'' can be obtained from the mirror-image, reflected in the wall, $\boldsymbol{v}'$ and p', of the given field by the formulas

$$u'' = u' - 2x\frac{\partial u'}{\partial x} + \frac{x^2}{\eta}\frac{\partial p'}{\partial x}, \tag{27a}$$

$$v'' = -v' - 2x\frac{\partial u'}{\partial y} + \frac{x^2}{\eta}\frac{\partial p'}{\partial y}, \tag{27b}$$

$$w'' = -w' - 2x\frac{\partial u'}{\partial z} + \frac{x^2}{\eta}\frac{\partial p'}{\partial z}, \tag{27c}$$

$$p'' = p' + 2x\frac{\partial p'}{\partial x} - 4\eta\frac{\partial u'}{\partial x}. \tag{27d}$$

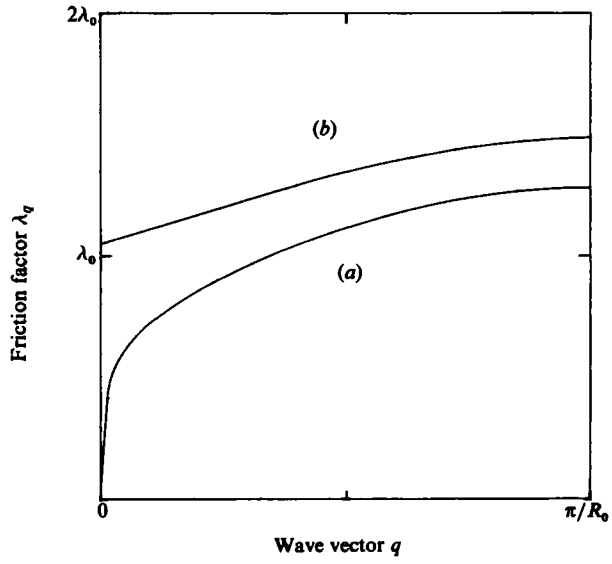

FIGURE 2. Friction factor for one-dimensional lattice (*a*) in an unbounded fluid and (*b*) near a wall. In the unbounded fluid, the drafting of one sphere behind another leads to a vanishing friction at long wavelengths, an unphysical result caused by the neglect of convective terms in the Navier–Stokes equations. In the presence of a wall, backflow imposed on the lattice causes a higher overall friction, and, more important, a non-vanishing value at $q = 0$. (Relative spacing $a/R_0 = 0.1$, relative distance $a/L = 0.4$.)

The new field also satisfies Stokes' equations and exactly cancels $\boldsymbol{v}$ on a planar surface at $x = 0$. Hence $\boldsymbol{v}''$ is the first reflected backflow field imposed by the stick boundary condition on the planar surface.

One could apply these formulas to the three-dimensional lattice result (11), but a more revealing exercise is to apply them to a simpler one-dimensional lattice velocity field. This may be constructed from the Oseen tensor $\boldsymbol{T}$ in the point-force approximation:

$$v^\beta(\boldsymbol{r}) = \sum_{n,\beta} T^{\alpha\beta}(\boldsymbol{r}) f_n^\beta, \tag{28}$$

where $T^{\alpha\beta}(\boldsymbol{r})$ is defined as $(8\pi\eta r)^{-1}(\delta^{\alpha\beta} + r^\alpha r^\beta/r^2)$. Let the lattice run in the z-direction with a lattice parameter R_0 and sphere diameter a, with only motion along z allowed. Without the wall, the Oseen tensor gives the unperturbed field

$$v = \frac{m_0}{8\pi\eta} \sum_{n,q} e^{\mathrm{i}qnR_0}\left[\frac{f_q}{r_n} + \frac{r_n(r_n \cdot f_q)}{r_n^3}\right], \tag{29}$$

which, after the application of approximate boundary conditions on the surfaces of the spheres and following the other procedures outlined in §2, gives the following friction factor:

$$\lambda_q = \lambda_0\left\{1 + 3\left(\frac{a}{R_0}\right)\sum_{m=1}^{\infty}\frac{1}{m}\cos(mqR_0) + O\left[\left(\frac{a}{R_0}\right)^3\right]\right\}^{-1}. \tag{30}$$

The sum can be performed exactly, revealing a logarithmic singularity at $q = 0$ (Glasser 1974):

$$\lambda_q = \lambda_0\left\{1 - 3\left(\frac{a}{R_0}\right)\ln\left[2\sin\left(\tfrac{1}{2}qR_0\right)\right]\right\}^{-1}. \tag{31}$$

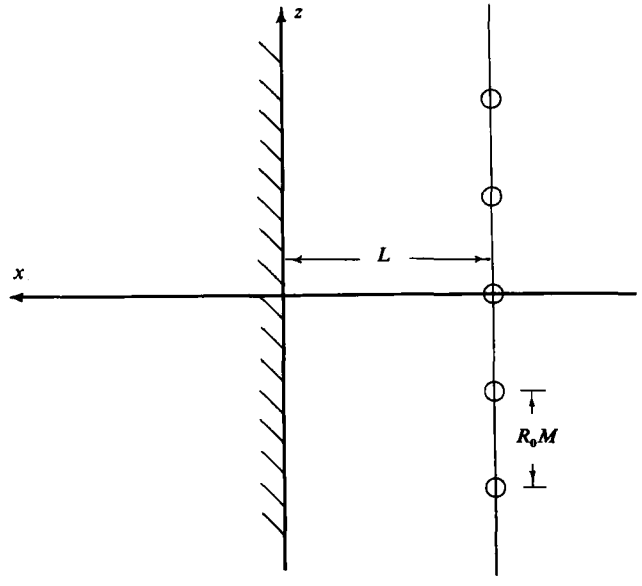

FIGURE 3. Geometry for one-dimensional lattice near a wall. Spheres of radius a are constrained to move longitudinally parallel to the wall in the direction $\hat{z}$, always remaining at a distance L from the wall.

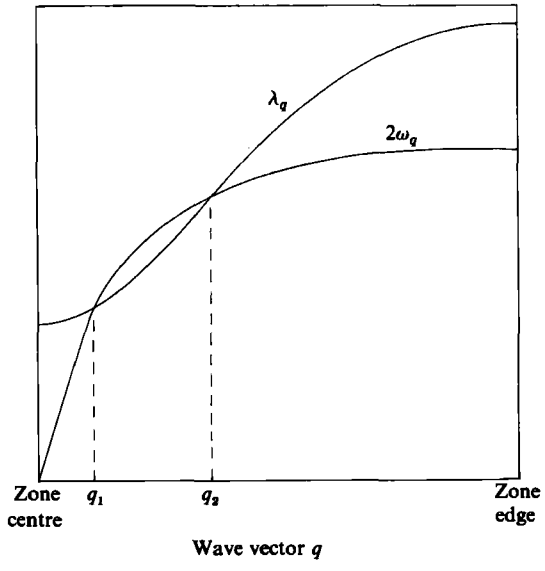

FIGURE 4. Schematic comparison of (a) transverse friction factor λ_q for a lattice bounded by walls, which has a non-zero value at the zone centre, and (b) twice the elastic dispersion curve $2\omega_q$, showing a situation in which propagating behaviour occurs in some range $[q_1, q_2]$ of non-zero wave vectors for which $\lambda_q < 2\omega_q$.

This singularity corresponds to a vanishing friction factor, seen in curve (a) of figure 2. The vanishing is a well-known result for the steady translation of an infinitely long rod along its axis in an unbounded fluid. For unsteady motion, inertial effects, which are neglected here, provide a finite resistance; thus in any physical situation no singularity can exist. Whatever the true friction factor, however, (31) suggests

that it is small, attributable to the lack of backflow and to the 'drafting' of one sphere behind another. Next we will see that the inclusion of backflow reflected from a wall leads to a dramatic increase in the friction.

Let the lattice be at a distance L from a parallel wall at $x = 0$ (see figure 3). The mirror-image field $\boldsymbol{v}'$ can be found from (31) by replacing

$$r_n^2(L) = (x+L)^2+y^2+(z-nR_0)^2$$

with $r_n^2(-L)$. The z-component of the backflow from the nth moving particle evaluated at the centre of the particle at z is found from (27c) to be

$$w'' = -\left[\frac{1}{r_n(-L)}+\frac{z-nR_0}{r_n^3(-L)}\right]+\frac{2x}{r_n^3(-L)}\left[L-3L\frac{(z-nR_0)^2}{r_n^2(-L)}\right], \tag{32}$$

and the new friction factor is

$$\lambda_q = \lambda_0\left\{1-\frac{9}{16}\frac{a}{L}+3\left(\frac{a}{R_0}\right)\sum_{m=1}^{\infty}\left[\frac{1}{m}-\frac{m^4+\epsilon^2m^2+\frac{3}{4}\epsilon^4}{(m^2+\epsilon^2)^{\frac{5}{2}}}\right]\cos mqR_0\right\}^{-1}, \tag{33}$$

where $\epsilon = 2L/R_0$. The $\frac{9}{16}a/L$ term is the well-known single-particle correction for motion parallel to a wall, and is the same for all normal modes. The more-interesting backflow correction term in the summand can be identified by comparing with (30). The previously divergent sum now converges at $q = 0$, where $\epsilon = 2L/R_0$, producing curve (b) of figure 2. In this case the friction factor shows less dispersion (less q-dependence) in the presence of a wall, and remains finite even when the wall is far away from the spheres.

The point of this exercise is that the friction for the shear modes of a colloidal crystal lattice confined to a thin cell will not vanish as they do in an infinite lattice, because the presence of walls imposes backflow. This is not to say that propagating modes cannot exist in a confined sample; they will still occur for whatever range of $\boldsymbol{q}$ in which the friction factor is small enough, i.e. $\lambda_q^\nu < 2w_q^\nu$. However, since w_q^ν vanishes at $q = 0$, shear modes can propagate only in some range of non-zero $\boldsymbol{q}$. This point is expressed schematically in figure 4.

6. Conclusions

The central result we have presented is an explicit calculation of the drag or friction factors for small oscillatory motions of a dilute *bcc* lattice of spheres in a viscous solvent. The formalism is based on classical solid-state analysis (Fourier transforms and small displacements), and is correct for short wavelengths, where the discreteness of the lattice is important, as well as for long wavelengths. We find that the hydrodynamic interaction enters at order $\phi^{\frac{1}{3}}$, making it more important in regular arrays than in disordered arrangements, and that the friction is a function of the normal-mode $\boldsymbol{q}$. In longitudinal modes of an infinite lattice, backflow arises as a response to pressure gradients, causing the friction to remain finite for all $\boldsymbol{q}$, whereas transverse modes in an infinite lattice have no backflow, leading to a vanishing friction at $\boldsymbol{q} = 0$.† Also, in elastic lattices such as colloidal crystals, the friction is small enough for propagating modes (sound waves) to exist at small wave vectors; the effective mass for such modes is seen to include the fluid mass carried along by the

† We wish to thank a referee for pointing out that the transverse-mode friction vanishes at $\boldsymbol{q} = 0$ only in the leading terms of order $\phi^{\frac{1}{3}}$; the next-higher-order terms of order ϕ do not vanish (Zuzovsky, Adler & Brenner 1983). These authors note the interesting fact that in the $\boldsymbol{q} = 0$ limit the results for random and ordered arrangements become identical.

particles. However, we have argued that in the presence of a wall, propagating modes, if they exist at all, will only occur in a range of wave vectors that does not include $q = 0$ because backflow imposed by the wall prevents the friction from vanishing.

We would like to thank Dr Wim van Saarloos for helpful discussions, correspondence and a preprints of his work. We are also grateful to Dr C. W. J. Beenakker for kindly supplying preprints of his work. Financial support for this work was provided by the Department of Energy Contract DE-AC02-82ER13004 with partial support from National Science Foundation Grant DMR 82-06472 (Noel Clark) and The Martin Fisher School of Physics, Brandeis University (Alan Hurd).

REFERENCES

Beenakker, C. W. J. & Mazur, P. 1984 *Preprint.*

Benzing, D. W. & Russel, W. B. 1981 *J. Coll. Interface Sci.* **83**, 178.

Glasser, M. L. 1974 *J. Math. Phys.* **15**, 188.

Goren, S. L. 1983 *J. Fluid Mech.* **132**, 185.

Happel, J. & Brenner, H. 1973 *Low Reynolds Number Hydrodynamics.* Noordhoff.

Hasimoto, H. 1959 *J. Fluid Mech.* **5**, 317.

Hurd, A. J. 1981 Ph.D. thesis, University of Colorado.

Hurd, A. J., Clark, N. A., Mockler, R. C. & O'Sullivan, W. J. 1982 *Phys. Rev.* **A26**, 2869.

Joanny, J. F. 1979 *J. Coll. Interface Sci.* **71**, 622.

Lindsay, H. M. & Chaikin, P. M. 1982 *J. Chem. Phys.* **76**, 3774.

Mazur, P. 1982 *Physica* **110A**, 128.

Mazur, P. & Bedeaux, D. 1974 *Physica* **76**, 235.

Mazur, P. & van Saarloos, W. 1982 *Physica* **115A**, 21.

Noble, B. 1969 *Applied Linear Algebra.* Prentice-Hall.

Pieranski, P., Dubois-Violette, E., Rothen, F. & Strzelecki, L. 1981 *J. Phys.* (*Paris*) **42**, 53.

Russel, W. B. & Benzing, D. W. 1981 *J. Coll. Interface Sci.* **83**, 163.

Saffman, P. G. 1973 *Stud. Appl. Math.* **52**, 115.

Saarloos, W. van & Mazur, P. 1983 *Physica* **120A**, 77.

Zuzovsky, M., Adler, P. M. & Brenner, H. 1983 *Phys. Fluids* **26**, 1714.